***Proceedings of the IASS 2024 Symposium***
*Redefining the Art of Structural Design*
August 26-30, 2024, Zurich Switzerland
Philippe Block, Giulia Boller, Catherine DeWolf,
Jacqueline Pauli, Walter Kaufmann (eds.)

# A Framework for Parametric Structural Design of Topological Interlocking Flat Vaults

Elena SHILOVA*, Nicolo BENCINI[1]

*Architect
ARB/RIBA London, UK; Ordem dos Arquitectos, Portugal
shilova.arch@gmail.com

[a] Associate Structural Engineer, London, UK
nicbencini@gmail.com

## Abstract

Topological Interlocking (TI) is a modular historic construction method of covering large spans with standardized components without connectors. The concept has now been revisited, following recent developments in parametric methods, resulting in algorithms capable of creating a large number of unique designs. However, due to structural complexities, only a few examples of TI have been embodied in mainstream permanent built projects. This paper therefore proposes a generalized framework for connecting the iterative digital design of TIs in combination with an assessment of structural integrity. The algorithm employs the principles of finite element methods to evaluate structural resilience in relation to various loading scenarios (i.e. deflections and stress), to suggest: firstly, the optimal span of the system; and secondly, the required boundary condition. This was tested on a set of small-scale 3d printed models, demonstrating that the framework creates a path beyond geometrical design, towards implementing TI into mainstream construction. It thus offers an approach to modular design focused on a sustainable circular economy.

**Keywords**: parametric structural analysis, kit of parts, topological Interlocking vaults, historical construction methods, modular construction, sustainable design.

## 1. Introduction.

### 1.1 Background. Definition of a 'Flat Vault'

The term Topological Interlocking (TI) or Topological Interlocking Assembly (TIA) describes systems in which a relatively large span is covered by discrete building components considerably smaller than the span itself. In addition, the blocks hold together reciprocally, by means of their geometrical interfaces, and without the use of connectors, fasteners or structural adhesives (Dyskin, Estrin et al. 2001 [1]).

The term '*Flat Vault*' refers to TIAs exhibiting behavior found in arched vaults (i.e. thrust) despite having no global curvature (Brocato and Mondardini 2014 [2]; Fantin, Ciblac and Brocato 2018 [3]; Gata et. al. 2019 [4]). This is achieved through the interlocking geometry of the blocks forming the vault, which rest upon one another, thus transferring the load of the system through compression and shear.

The Flat Vaults designed by Abeille, Truchet and Frézier (Frézier 1738 [5]) marked significant milestones in the history of topological interlocking, together with historical examples, including the Escorial Monastery, Cádiz and Lugo's Cathedral, along with Pontón de la Oliva (Gata et. al. 2019 [4]).

*1.1.1 Implementation of topological interlocking in contemporary design practice.*

*Copyright © 2024 by Elena Shilova and Nicolo Bencini*
*Published by the International Association for Shell and Spatial Structures (IASS) with permission.*

The contemporary notion of topological interlocking has been derived from material science, so adding rule-based logic into methods of creating new interlocking designs (Dyskin, Estrin et al. 2001 [1]; Dyskin, Estrin et al. 2001 [6]). Researchers employed modern developments in computation to create a variety of form-finding tools, ensuring an expansion of the library of topological interlocking designs (Weizmann, Amir and Grosman 2015 [7]). This resulted in permanent buildings (AAU Anastas, 2017, 2018 [8]), as well as full-scale architectural installations (Fallacara and Barberio 2018 [9]).

The TI method avoids concentrated stress in joints, which is advantageous for quasi-brittle materials (i.e. concrete, ceramics, and stone) that remain ubiquitous in the construction sector (Estrin, Dysking et al. 2011 [10]). The segmentation approach offers a viable alternative to monolithic construction, being potentially more resilient to impact, as well as proving tougher and stronger, and offering simplified logistics, recycling and reuse (Dyskin, Estrin et al. 2001 [6], Dyskin, Estrin et al. 2003 [23], Dyskin, Estrin et al. 2003 [24], Estrin, Dyskin, Pasternak 2011 [10]).

However, despite these benefits, there are a number of challenges when it comes to implementing TI in practice. This discretized approach increases fabrication complexity and relies on bespoke assembly sequences (Rippman and Block 2013 [11]); it is less familiar to the construction market, it requires complicated fabrication, contractor tendering, and compliance with building regulations. Furthermore, when it comes to regulatory compliance, the primary issues consist of the structural safety and stability of unreinforced Tas, in particular when implemented as self-supporting or load-bearing elements in a building (i.e. walls, roofs and floor slabs).

### *1.1.2 Problem Statement*

Several methods have been developed to evaluate the structural performance of TIA, involving Finite Element Analysis (FEM) (Short and Siegmund 2019 [12]; Laudage, Guenther, Siegmund 2023 [13]; Brocato and Mondardini 2014 [14]), and a force network method (Fantin, Ciblac and Brocato 2018 [3]). These are considered an ‘offspring’ of thrust network analysis (O’Dwyer 1999 [14]; Block and Ochsendorf 2007 [15).

Despite demonstrating undisputable precision and fidelity, the implementation of FEM modelling is relatively complex within a desired iterative design tool. This raises difficulties in the absence of a continuous feedback loop between the geometrical and structural design, enabling the designer to make an informed decision with regards to the practical implementation of TIA.

This led to the following research question: Can a parametric analysis tool based on a simplification of TIA structural behavior enable iterative design of such systems for architectural application? To address this issue, we propose a form-finding and parametric analysis method to structurally test TIA designs (see Figure 1). This involves a simplification of the complex interaction between the blocks down to a linear finite element model, capable of approximating the behavior of the overall system. This tool can then be used in the early design stages, i.e. prior to the project reaching maturity and the undertaking of main decisions on building construction systems.

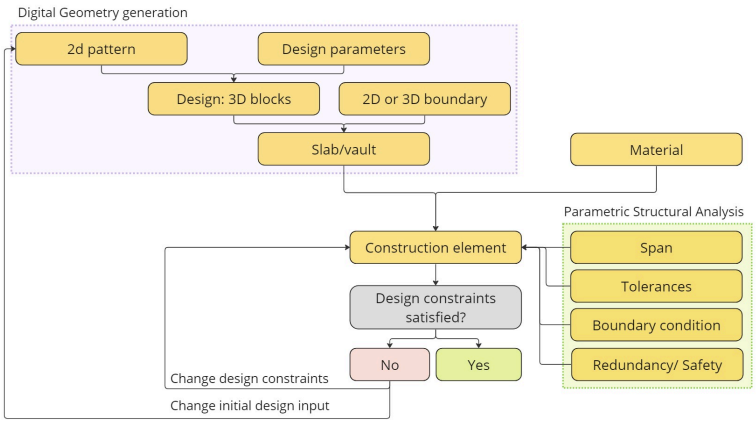


Figure 1: Proposed parametric design-analysis feedback loop

## 2. Methods

### 2.1 Digital design tool for Topological interlocking Assemblies.

When drawing up the digital design of the TI, we developed a custom algorithm using Spatial Slur half edge meshes by Reeves (2016 [16]) in Rhino 3D and Grasshopper (see Figure 2). The methodology followed the framework of creating a 3-dimensional TI from the base pattern and tilted planes, as described by Kanel-Belov, Dyskin et al. (2009 [17]), and employed by Shilova, Watts et al. (2023 [18]). The toolkit is available as a digital repository [25], available for free public use.

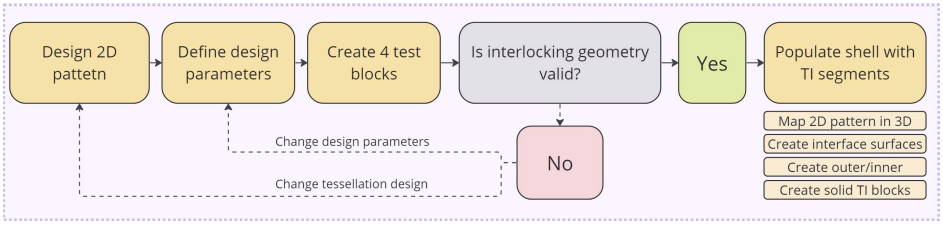


Figure 2: Digital Geometry generation workflow

*2.1.1 2D Base pattern generation and sorting.*

In this method, the designer initially created a 2d pattern in a repeated tile, following best practice rules to ensure the algorithm returned valid geometry (i.e. closed without non-manifold and open edges). The rules were then defined by the authors by testing a digital tool through a series of workshops (Shilova, Watts et al. 2023 [18]; Shilova, Murugesh and Weinstock 2018 [18]; AAG 2020 [21] and 2018 [20]), and by incorporating observations by Weizmann et al. (2015 [7]) and Tessmann (2012 [22]).

As a second step, each closed polygon in the pattern was given a separated layer. Open boundaries belonging to a single block at the tile's edges were assigned the same layer, and automatically joined into closed polygons by the algorithm. This resulted in the algorithm creating a continuous pattern of sorted closed polygons, ready to be used as an input to generate 3-dimensional components.

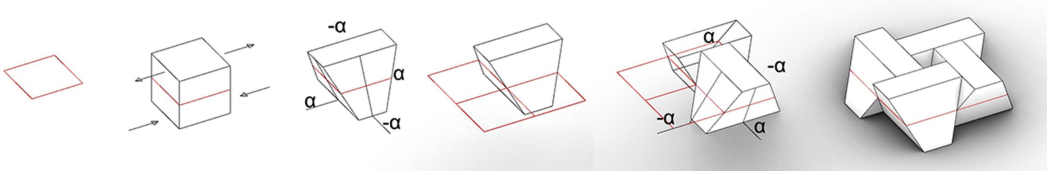


Figure 2: Method of creating an interlocking block 2x2 sample from a 2D tessellation pattern.

*2.1.2* Generation of 3-dimensional Topological Interlocking.

In the following step, the designer converted the 2d pattern into 3d geometry. Although his study only showed planar TIA, the digital tool was also built to cater for 3D shells (Shilova, Watts et al. 2023 [18]). Once the pattern was mapped, the algorithm created a set of tilted planes with alternating angles α and -α on each projected polygon, so establishing the interfaces of the future TIA blocks. Then, if valid geometry was found to have been generated on a test 2x2 assembly (see Figure 2), the desired pattern was mapped on the full desired surface, using the parallel projections method. Lastly, the shell depth defined the capping inner and outer faces of each solid block (see Figure 3).

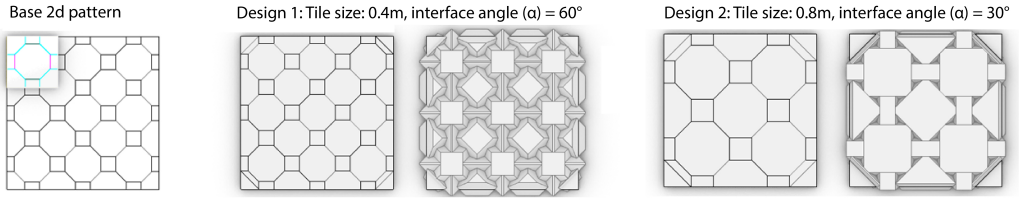


Figure 3: Generation of full TI from mapped pattern, using depth and inclination parameters.

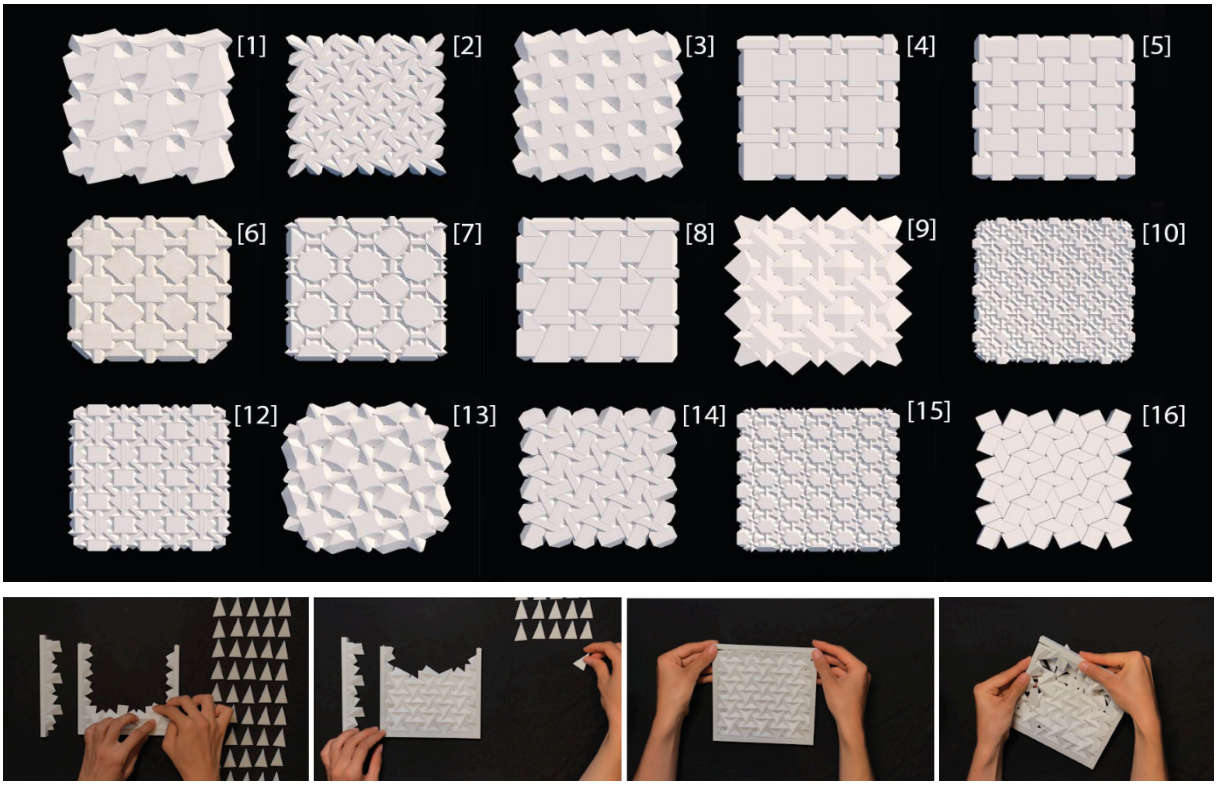


Figure 4: Top: Catalogue of generated TI assemblies. Bottom: Physical models to validate digital designs

### 3.1 Parametric Structural analysis tool for Topological interlocking Assemblies

Once the 3d geometry (see Figure 5) was developed by means of a digital design tool, the analytical model was created to simplify the interaction between the topological interlocking of the blocks to a linear finite element model.

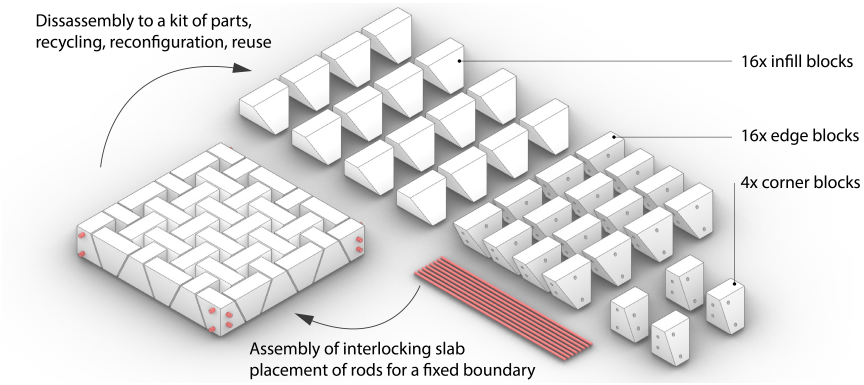


Figure 5: Topological interlocking design with truncated tetrahedra elements, used to develop parametric structural analysis tool. Section of the system shown in Figure 6.

#### 3.1.1 Generation of analytical model

This simplification was based on research by Laudage, Guenther and Siegmund (2023 [13]) and completed by representing the system as an arch, with all blocks in compression forming a compressive strut. This then converged on the central interlocking block acting as a pivot. The design of this truss undertakes minor adjustments in relation to the type of pattern, and the way the surfaces of the blocks interface. However, the overall logic remained the same. The points of rotation between the central block and the rest of the system were modelled as hinges, to allow for rotation mimicking the movement of blocks at the centre of the slab.

This arrangement allowed for the simplification of a complex block model to a finite element analytical model made up of three finite elements, forming an arch constrained within the depth of the slab (see Figure 6). The steel rod within the linear arrangement of blocks that tied the system together (See Figure 10, right) was then modelled as a continuous member connecting both ends of the arch and the arch. To assess the arch as a simply supported beam, a pinned support was applied at one end, then a sliding support was added to the other.

This model of a singular arch was subsequently assembled into a 3D representation of the system, with the intersecting orthogonal arches connected at the points of interaction. This allowed for an approximation of the 3D behavior of the interlocking slab for the chosen pattern, so permitting the compounding deflections to be captured by means of a singular representation.

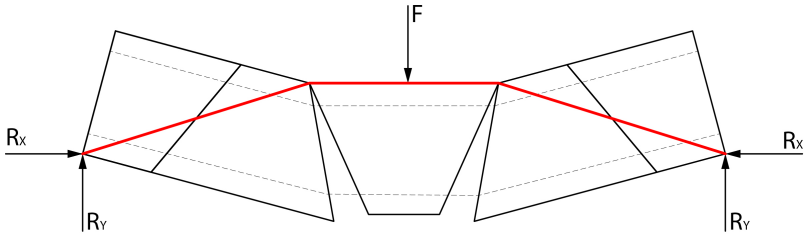


Figure 6. Schematic section, illustrating the principle of Mises truss along the force network to represent the deflection response in the TI. After Laudage, Guenther and Siegmund (2023 [13]); adapted to specific Abeille geometry (3x3 loose blocks configuration) by the authors

The analytical model for the system was built using a combination of Python and Grasshopper (Rhino) to translate geometrical, material loading and constraint information into a stiffness matrix representing the structural system. By maintaining full control over the creation, and resolution of the stiffness matrix, the team was able to implement logic scenarios capable of more accurately mimicking the behavior of topological interlocking. Specifically, once an arch member deflected past a certain point and outside of the depth of the block, then this arrangement of blocks would no longer be in compression and cease to act as a connected arch. It was therefore removed from the system. This flexibility allowed for a more accurate representation of the system, as well as more control over which members contributed to the interlocking.

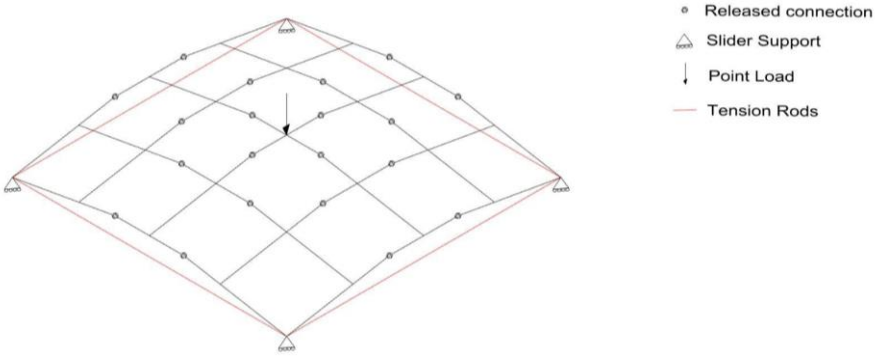


Figure 7. Diagram showing model setup

The edge condition of the slab was modelled with one pinned support and three sliding supports allowing for free movement in the x and y axis. These supports were connected with linear members representing the rods placed along the edge members, thus ensuring that the outward movement of the edge supports would be tied back by these rods. This represented the edge condition of the physical model, which had rods around the perimeter to hold the blocks in place. The final analytical model also contained rods holding the central block in place, which were added to the physical model in order to reduce slippage between the blocks.

### 4.1 Analysis

The model was built within Rhino, with the geometrical data, materials, section properties and constraints all assembled into a global [Kp] stiffness matrix representing the overall system. From this, a structural stiffness matrix [Ks] was obtained by removing the rows and columns corresponding to nodes fixed at supports.

The load was applied as a point load to the central block of the system and compiled into a force vector {p}, then multiplied by the inverse of the structural stiffness matrix [Ks] to obtain the displacement vector {d} representing the deflections of the system. This resulted in a vector containing a value for the displacement, or rotation, for each degree of freedom for each support. All other structural results were then derived from the displacement vector. Furthermore, if an arch member deflected past the point at which it would be beneficial to the system, this was captured and removed from the global stiffness matrix, with the solution subsequently recalculated [26].

$$[Ks]^{-1}\{p\} = \{d\} \qquad (1)$$

The results from the analysis were tabulated to determine whether the system as a whole remained within the permissible limits under the different loading scenarios, so ensuring that all members remained acting in compression. The axial forces within the steel rods were also obtained from the change in length of the rods, being used to determine the size of rod sufficient to tie the edges of the slab together.

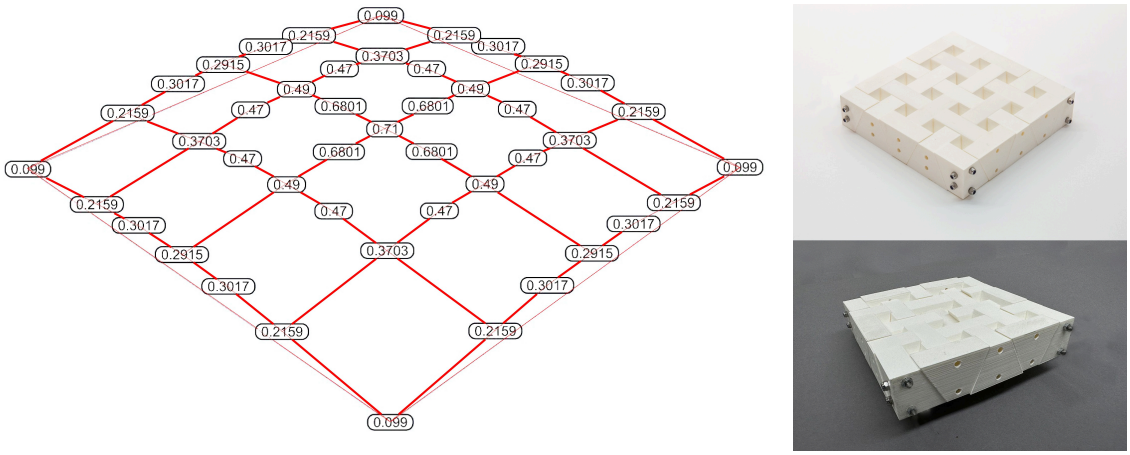


Figure 8: Left: Digital model results. Right: 3x3 physical model before and after 70kg load testing

### 4.1 Physical prototyping to validate digital structural analysis tool.

Physical testing was conducted on a series of 3d printed models, both of linear interlocking 3x1 (n=3), 4x1 and 5x1 ‘arches’ and 3x3 (n=9), 4x4 (n=16) and 5x5 (n=25) square slabs, where n corresponded to the number of unreinforced infill blocks, excluding the boundary blocks fixed via double layer of rods. All prototypes used identical 30mm (h) x 47mm (w) x 47mm (l) truncated tetrahedra with a 25° side angle for the interlocking infill, while using half-tetrahedral geometries for the edges and quarters for the corners. In addition, the interlocking pattern was based on a square grid and selected due to its simplicity, as well as historical precedents. The block geometry and dimensions are shown in Figure 5. The linear ‘arches’ and the boundary blocks of the ‘slabs’ were held together by a double layer of 3mm steel rods, fixed at the ends by a double hex nut. The location of the rods was symmetrical to the centroid of the block. Moreover, the 3d printing was completed in PLA on Ultimaker 3 with the following settings: wall thickness: 1mm; infill density: 90%; infill line distance 0.47mm; gyroid infill pattern and 0.1mm infill layer.

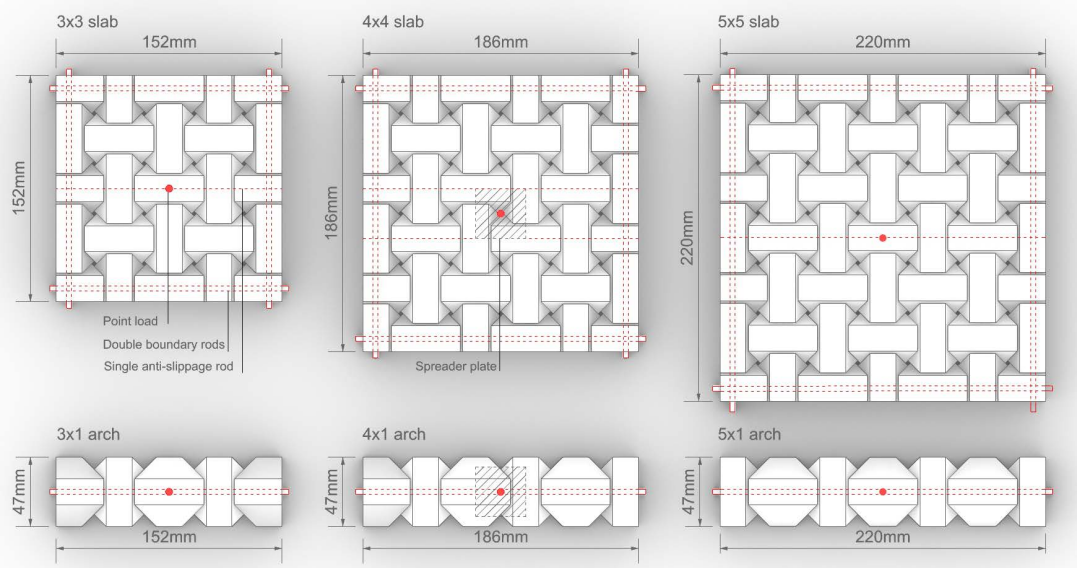


Figure 9: 3d Printed prototypes physically tested under a point load

### 2.2 Force-Displacement Experiments

The force-displacement response of the 3d printed prototypes was measured by a machine equipped with a tool to transmit the point load (see Figure 8). Firstly, the tool positioning was calibrated to touch the prototype surface without exerting pressure. Secondly, the 3d printed prototype was positioned on a raised frame, sized to provide support only under the fixed boundary of the prototype, thus leaving the unreinforced blocks cantilevering. Thirdly, the frame and prototype were placed on a weight scale (0.01 kg increment), with a clock gauge positioned above the prototype, and the stem positioned at the centre block where the point load was applied. Fourthly, the machine was programmed to inflict increasing deformation of the middle of the prototype with 0.01 mm increment, transmitting pressure on the weight scale. Finally, a camera recorded the experiments, simultaneously registering the dial of the gauge and the weight scale screen, until the limit of 100kg load or the failure of the prototype was reached. This approach registered continuous changes in the force-deformation pattern by matching the data of the clock gauge as opposed to the scales (see Appendix).

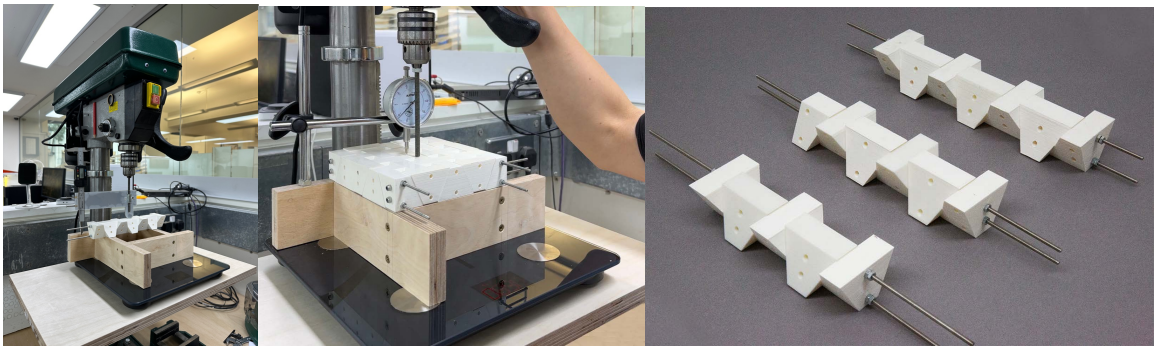

Figure 10. Left: Force vs Displacement tests set-up. Right: Single-arch 3x1, 4x1 and 5x1 prototypes

## 3. Results

The three, four and five block arch arrangements (as shown in figures 9 and 10) were tested first, with the deflections from these models under loading increments of 5kg plotted and compared to the results obtained from the digital studies. These results were then employed to calibrate the analytical model results to better match the deflections, while the following graphs were plotted to compare the behaviors. It was observed that the physical and digital models followed a very similar rate of

deflection under loading, with the physical model only deflecting slightly less than the digital model. However, since it was generally within +/- 1mm, this was deemed to be within acceptable tolerances (Figure 11).

This information was then used to calibrate the 3x3, 4x4 and 5x5 slab analytical models, and the results were plotted in the graph below (Figure 12). In addition, an additional rod was added to the system to hold the central block in place and so avoid any slippage of the blocks (Figure 9).

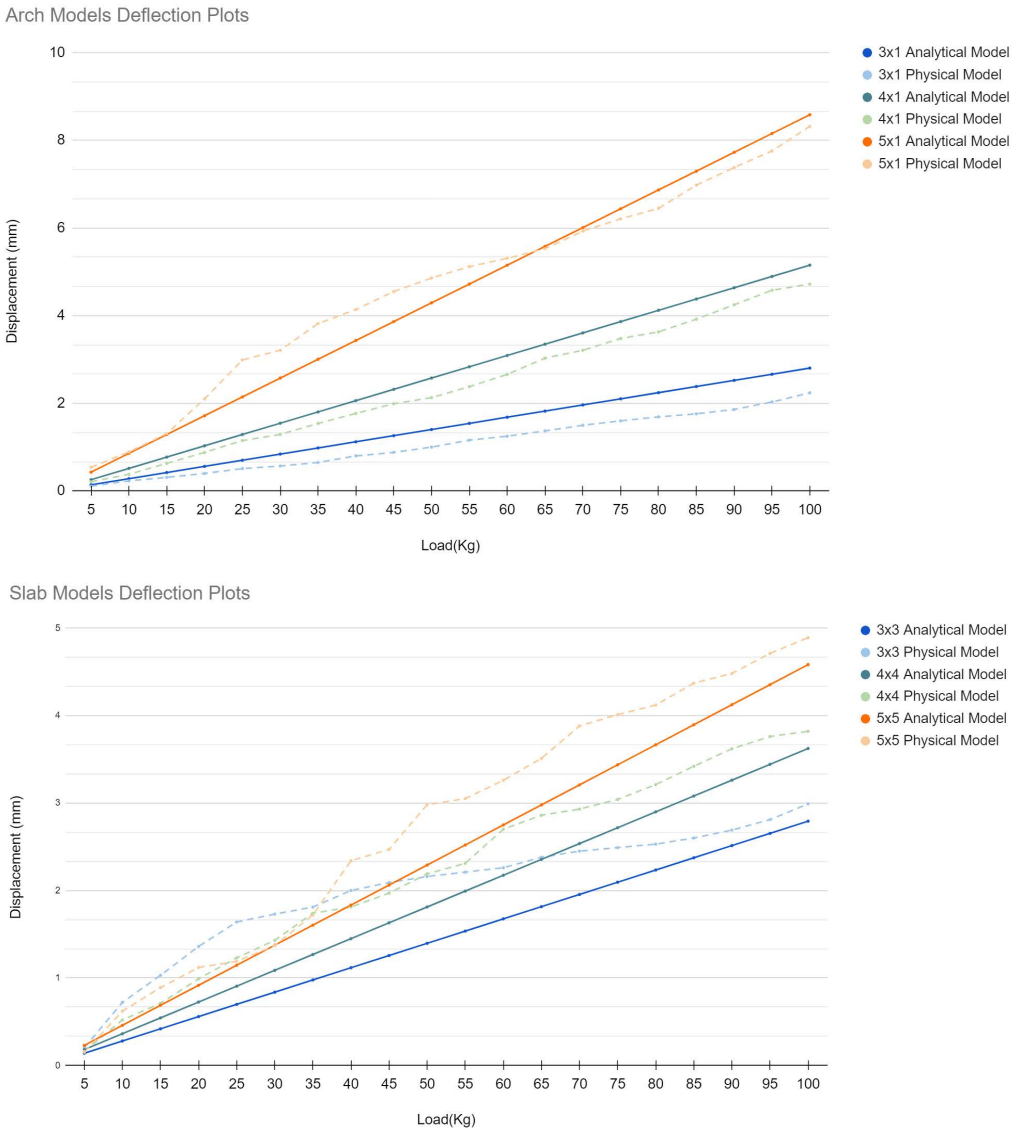


Figure 11. Top: 3x1, 4x1, 5x1 arch models force-deflection comparison: digital vs physical models. Bottom: 3x3, 4x4, 5x5 slab models force-deflection comparison: digital vs physical models

The physical results showed an area of higher deflections for the first few load applications, which then converged and aligned with the deflections calculated in the digital model. This was consistent among all three of the slab tests, most likely due to slippage and rearrangement of the blocks as the initial load was applied, until the system settled into a stable 'locked' state. From this point, it started to exhibit linear deformation increases that matched the results obtained from the digital studies.

### 3.1 Potential architectural application and future discussion

This study has indicated that this approach forms a step towards a simplified structural verification that will assist designers in practical implementation of TIAs, as well as leveraging their benefits in

comparison to monolithic systems. However, certain critical topics have not been addressed in this paper, including: (1) tolerances; (2) logistics; (3) assembly; (4) cost; ad (5) integration with other load-bearing building systems.

According to Short and Siegmund (2019 [12]), TIA outperforms equivalent size monolithic plates in terms of toughness for the majority of the strength modulus ratio materials and low strength blocks. This ability to work with blocks of lower strength highlights the potential for combining TIA with sustainable materials such as stone, terracotta or bio-based materials (i.e. hemp mixes). Therefore, the benefits of the system cannot be evaluated solely within the structural domain, but must rather rely on a material implementation and larger scale. The authors therefore aim to address these aspects by means of future research. In addition, additional research into strategies relating to disassembly, recycling and reuse would strengthen the advantages of TIAs as forming a viable system facilitating circular economy goals in the construction sector.

## 4. Conclusion

This paper has provided a generalized framework for the geometrical design and structural validation of topological interlocking Flat Vaults. In addition, it has focused on an analysis model for force-deflection response in linear and two-dimensional systems of truncated polyhedra, derived from historical Abeille design. Overall, these results have revealed that the simplified analytical model provides an accurate representation of the behavior of the interlocking system, and is therefore capable of being used as a simplified approach to model complex interlocking behavior. However, it should be noted that this does not account for any movements due to the redistribution, or slipping, of components, and is therefore only beneficial for modelling fully locked systems. Thus, in most practical cases where the system would be tightened to the extent that all members are fully locked and function as a unified slab, the proposed analytical approach could be used to model the system. This highlights that it is imperative to undertake further testing with larger-scale prototypes to determine the use of the method on an architectural scale.

## Acknowledgements

The team expresses deep gratitude to Thomas Siegmund for his guidance in developing the structural analysis tool, along with Philip Singer and Taole Chen for their contributions to the digital design tool, and Yuri Estrin for his mentorship. Furthermore, the team wishes to offer thanks to Rihards Saknitis for the photography and Robert Sims for model-making support.

## References

[1] A.V Dyskin, Y. Estrin, A.J. Kanel-Belov and E. Pasternak. “Toughening by Fragmentation. How topology helps?” *Advanced Engineering Materials*, 3, Issue 11, 885-88. 2001

[2] M. Brocato and L. Mondardini. “Parametric analysis of structures from flat vaults to reciprocal grids”, *IJAC.* 2014

[3] M. Fantin, L. Mondardini, and M. Brocato. “Resistance Of Flat Vaults Taking Their Stereotomy Into Account”. *Journal Of Mechanics of Materials and Structures*, Vol. 13, No. 5, 2018

[4] M. Gata, Moreno, K. Mueller, Caitlin and V. Ernesto. “Designing strategies for Topological Interlocking Assemblies in architecture. Flat Vaults”. *Conference: IASS 2019: FORM and FORCE*, Barcelona. October 2019

[5] A. Frézier, A. *La théorie et la pratique de la coupe des pierres. Traité de stéréotomie à l'usage de l'architecture.* A Paris: chez Charles-Antoine Jombert, [1754-1769]. ETH-Bibliothek Zürich. 1738

[6] A.V Dyskin, Y Estrin, A.J. Kanel-Belov, and E. Pasternak. “Toughening by fragmentation. How topology helps?” *Advanced Engineering Materials*, 3, Issue 11, 885-888. 2001

[7] M. Weizmann, O. Amir, and J. Grobman. “Topological Interlocking in Architectural Design”. *CAADRIA* 2015, 107-116, 2015.

[8] AAU Anastas, *The Flat Vault. Stone Matter*s (2017). AAU Anastas, 2018 Accessed 12.01.2024 at: https://aauanastas.com/projects/ 2018

[9] G. Fallacara and M. Barberio. “An Unfinished Manifesto for Stereotomy” 2.0. *Nexus Netw J* 20, 519–543 (2018). https://doi.org/10.1007/s00004-018-0390-z 2018

[10] Y. Estrin, A.V. Dyskin, E. Pasternak, "Topological as a material design concept". In*: Materials Science and Engineering*, pp. 1189–1194, 2011
[11] M. Rippmann, and P. Block, "Rethinking structural masonry: Unreinforced, stone-cut shells". *Proceedings of the ICE - Construction Materials.* 166. 378-389. 2013
[12] M. Short and T. Siegmund. "Scaling, Growth, and Size Effects on the Mechanical Behavior of a Topologically Interlocking Material Based on Tetrahedra Elements". *J. of Applied Mechanics* 86, 2019
[13] S. Laudage, E. Guenther and T. Siegmund. "Design and analysis of a lightweight beam-type topologically interlocked material system". *Structures.* 51. 1402-1413. 10.1016/j.istruc.2023.03.126.
[14] D. O'Dwyer. "Funicular analysis of masonry vaults", *Comput. Struct.* 73:1-5, 1999, 187–197.
[15] P. Block and J. Ochsendorf. "Thrust network analysis: a new methodology for three-dimensional equilibrium", *J. IASS* 48:3, 167–173. 2007
[16] D. Reeves. "Spatial Slur" https://spatialslur.gitlab.io/docs/api/index.html
[17] A. Kanel-Belov, A. Dyskin, Y. Estrin, E. Pasternak, I. Ivanov-Pogodaev. (2009). Interlocking of Convex Polyhedra: towards a Geometric Theory of Fragmented Solids. *Moscow Mathematical Journal.* 10. 10.17323/1609-4514-2010-10-2-337-342.
[18] E. Shilova, A. Watts, B. Ayati, A. Chandler, A. Gutierrez Rivas. Bridging The Gap Between Academia and Practice: A case study for collaborative digital design to fabrication workflow for interlocking kit-of-parts. *Proceedings of the eCAADe 41*, Volume 2, pp 29-38. 2023.
[19] E. Shilova, M. Murugesh, and M. Weinstock. *Robotic Fabrication of Segmented Shells: Integrated Data-Driven Design. Conference: Proceedings of the Symposium on Simulation for Architecture and Urban Design*, 20, pp205-212, 2018.
[20] E. Shilova and T. Chen. "Interlocking-based Robotic Fabrication of Segmented Shells". *Advances in Architectural Geometry 2018* www.architecturalgeometry.org/aag18/workshop-15-interlocking-based-robotic-fabrication/, accessed 26. 03.2024
[21] E. Shilova, M. Aceytuno Poch, and T. Chen, Sustainable strategies for robotic fabrication of segmented shells. *Advances in Architectural Geometry 2020* www.aag2020.com/recycled, accessed 26. 03.2024
[22] O. Tessmann. Topological Interlocking Assemblies. Digital Applications in Construction, *eCAADe* 30, 211-219.2012
[23] A. Dyskin, Y. Estrin, A. Kanel-Belov, and E. Pasternak. A new principle in design of composite materials: reinforcement by interlocked elements. *Composites Sciene and Technology* 63,483–491 , 2003
[24] A. Dyskin, A., Y. Estrin, E. Pasternak, H. Khor, and A. Kanel-Belov. Fracture Resistant Structures Based on Topological Interlocking with Non-planar Contacts. *Advanced Engineering Materials* 5, 116–119, 2003
[25] Digital tookit available at https://github.com/Abstractmachina/topological_interlocking_vaults
[26] H. P. Gavin. "Frame Element Stiffness Matrices" Matrix Structural Analysis, 2012.

## Appendix. Structural analysis and physical experiments data.

| | Displacement (mm) | | | | | | | | | | |
|---|---|---|---|---|---|---|---|---|---|---|---|
| | 3x1 Arch | | 4x1 Arch | | 5x1 Arch | | 3x3 Slab | | 4x4 Slab | |
| Load (Kg) | 3x1 Analytical Model | 3x1 Physical Model | 4x1 Analytical Model | 4x1 Physical Model | 5x1 Analytical Model | 5x1 Physical Model | 3x3 Analytical Model | 3x3 Physical Model | 4x4 Analytical Model | 4x4 Physical Model |
| 5 | 0.1 | 0.11 | 0.3 | 0.21 | 0.4 | 0.54 | 0.1 | 0.2 | 0.2 | 0.16 |
| 10 | 0.3 | 0.23 | 0.5 | 0.38 | 0.9 | 0.89 | 0.3 | 0.72 | 0.4 | 0.52 |
| 15 | 0.4 | 0.31 | 0.8 | 0.63 | 1.3 | 1.31 | 0.4 | 1.03 | 0.5 | 0.71 |
| 20 | 0.6 | 0.4 | 1.0 | 0.88 | 1.7 | 2.1 | 0.6 | 1.36 | 0.7 | 0.99 |
| 25 | 0.7 | 0.51 | 1.3 | 1.15 | 2.1 | 2.99 | 0.7 | 1.64 | 0.9 | 1.23 |
| 30 | 0.8 | 0.57 | 1.5 | 1.29 | 2.6 | 3.21 | 0.8 | 1.73 | 1.1 | 1.43 |
| 35 | 1.0 | 0.65 | 1.8 | 1.54 | 3.0 | 3.82 | 1.0 | 1.81 | 1.3 | 1.74 |
| 40 | 1.1 | 0.8 | 2.1 | 1.77 | 3.4 | 4.14 | 1.1 | 2 | 1.4 | 1.81 |
| 45 | 1.3 | 0.88 | 2.3 | 1.99 | 3.9 | 4.55 | 1.3 | 2.09 | 1.6 | 1.97 |
| 50 | 1.4 | 1 | 2.6 | 2.13 | 4.3 | 4.86 | 1.4 | 2.16 | 1.8 | 2.19 |

| | Displacement (mm) | | | | | | | | | |
|---|---|---|---|---|---|---|---|---|---|---|
| | 3x1 Arch | | 4x1 Arch | | 5x1 Arch | | 3x3 Slab | | 4x4 Slab | |
| Load (Kg) | 3x1 Analytical Model | 3x1 Physical Model | 4x1 Analytical Model | 4x1 Physical Model | 5x1 Analytical Model | 5x1 Physical Model | 3x3 Analytical Model | 3x3 Physical Model | 4x4 Analytical Model | 4x4 Physical Model |
| 55 | 1.5 | 1.16 | 2.8 | 2.38 | 4.7 | 5.12 | 1.5 | 2.21 | 2.0 | 2.31 |
| 60 | 1.7 | 1.25 | 3.1 | 2.66 | 5.2 | 5.31 | 1.7 | 2.26 | 2.2 | 2.7 |
| 65 | 1.8 | 1.37 | 3.3 | 3.03 | 5.6 | 5.53 | 1.8 | 2.38 | 2.4 | 2.86 |
| 70 | 2.0 | 1.5 | 3.6 | 3.21 | 6.0 | 5.93 | 2.0 | 2.45 | 2.5 | 2.93 |
| 75 | 2.1 | 1.6 | 3.9 | 3.48 | 6.4 | 6.21 | 2.1 | 2.49 | 2.7 | 3.04 |
| 80 | 2.2 | 1.69 | 4.1 | 3.63 | 6.9 | 6.45 | 2.2 | 2.53 | 2.9 | 3.21 |
| 85 | 2.4 | 1.76 | 4.4 | 3.92 | 7.3 | 6.98 | 2.4 | 2.6 | 3.1 | 3.42 |
| 90 | 2.5 | 1.86 | 4.6 | 4.25 | 7.7 | 7.38 | 2.5 | 2.69 | 3.3 | 3.62 |
| 95 | 2.7 | 2.03 | 4.9 | 4.58 | 8.2 | 7.76 | 2.7 | 2.81 | 3.4 | 3.76 |
| 100 | 2.8 | 2.24 | 5.2 | 4.72 | 8.6 | 8.32 | 2.8 | 2.99 | 3.6 | 3.82 |